PRACTICAL APPROACH SERIES
Series Editor: B. D. Hames

This book is unique in providing current experimental methods for research on the cytoskeleton and its relationships to signalling and cell regulation. Thus, it bridges two extremely active and fertile areas of research. The focus is directed particularly towards methods based on recent advances in molecular biology, microscopy and immunology. A second emphasis is on methods for understanding dynamic changes in cells. A third emphasis is on the formation and turnover of macromolecular and supramolecular complexes, which are so important in driving cell regulation and the behaviour of cytoskeletal elements. In each case, the method is presented as a step-by-step protocol with full accompanying practical advice. The authors are all active researchers in the field with a wealth of knowledge about the best methods available and how to use them most effectively. The result is a practical manual that also serves as a valuable reference companion; it will be equally thumbed in the lab and the office!

OXFORD

ISBN 0-19-963781-4

CARRAWAY and CARRAWAY

Cytoskeleton: signalling and cell regulation

OXF

Cytoskeleton: signalling and cell regulation

PRACTICAL APPROACH

Edited by
K. L. CARRAWAY and C. A. C. CARRAWAY

The Practical Approach Series
Series Editor: B. D. Hames

25. Chomczynski, P. and Sacchi, N. (1987). *Anal. Biochem.*, **162**, 156.
26. Pardue, M. L. and Gall, J. G. (1969). *Proc. Natl. Acad. Sci. USA*, **64**, 600.
27. Aigner, S. and Pette, D. (1990). *Histochemistry*, **95**, 11.
28. Veyrune, J.-L., Campbell, G. P., Wiseman, J. W., Blanchard, J.-L., and Hesketh, J. E. (1996). *J. Cell Sci.*, **109**, 1185.
29. Mahon, P., Beattie, J. H., Glover, L. A., and Hesketh, J. E. (1995). *FEBS Lett.*, **373**, 76.
30. Sambrook, I., Fritsch, E. F., and Maniatis, T. (ed.) (1989). *Molecular cloning: a laboratory manual.* Cold Spring Harbor Laboratory Press, NY.
31. Zehner, Z. E., Shepherd, R. K., Gabryszuk, J., Fu, T.-F., Al-Ali, M., and Holmes, W. M. (1997). *Nucleic Acids Res.*, **25**, 3362.
32. White, K. N. and Fu, L. (1995). *Methods Mol. Cell. Biol.*, **5**, 222.
33. Tautz, D., Hulskamp, M., and Sommer, R. J. (1992). In *In situ hybridization: a practical approach* (ed. D. G. Wilkinson). IRL Press, Oxford.
34. Pomeroy, M. E., Lawrence, J. B., Singer, R. H., and Billings-Gagliardi, S. (1991). *Dev. Biol.*, **143**, 58.
35. Cripe, L., Morris, E., and Fulton, A. B. (1993). *Proc. Natl. Acad. Sci. USA*, **90**, 2724.
36. Morris, E. J. and Fulton, A. B. (1994). *J. Cell Sci.*, **107**, 377.
37. Non-radioactive *in situ* hybridization application manual. Boehringer Mannheim.
38. Cohen, N. S. (1996). *J. Cell. Biochem.*, **61**, 81.
39. Braissant, O. and Wahli, W. (1998). *Boehringer Mannheim Biochem.*, **1**, 10.
40. Long, R. M., Singer, R. H., Meng, X., Gonzales, I., Nasmyth, K., and Jansen, R.-P. (1997). *Science*, **277**, 383.
41. Femino, A. M., Fay, F. S., Fogarty, K., and Singer, R. H. (1998). *Science*, **280**, 585.
42. Kislauskis, E. H., Li, Z., Taneja, K. L., and Singer, R. H. (1993). *J. Cell Biol.*, **123**, 165.
43. Kislauskis, E. H., Xiaochun, Z., and Singer, R. H. (1994). *J. Cell Biol.*, **127**, 441.
44. Wiseman, J. W., Glover, A., and Hesketh, J. E. (1997). *Int. J. Biochem. Cell Biol.*, **29**, 1013.
45. Wiseman, J. W., Glover, A., and Hesketh, J. E. (1997). *Cell Biol. Int.*, **21**, 243.
46. Goldspink, P. H., Sharp, W. W., and Russell, B. (1996). *J. Cell Sci.*, **110**, 2969.
47. Gossen, M., Freunlieb, S., Bender, G., Muller, G., Hillen, W., and Bujard, H. (1995). *Science*, **268**, 1766.
48. Hoek, K. S., Kidd, G. J., Carson, J. H., and Smith, R. (1998). *Biochemistry*, **37**, 7021.
49. Ross, A. F., Oleynikov, Y., Kislauskis, E. H., Taneja, K. L., and Singer, R. H. (1997). *Mol. Cell. Biol.*, **17**, 2158.
50. SenGupta, D. J., Zhang, B., Kraemer, B., Pochart, P., Fields, S., and Wickens, M. (1996). *Proc. Natl. Acad. Sci. USA*, **93**, 8496.

11

Cell shape control and mechanical signalling through the cytoskeleton

WOLFGANG H. GOLDMANN, JOSÉ LUIS ALONSO, KRZYSZTOF BOJANOWSKI, CLIFFORD BRANGWYNNE, CHRISTOPHER S. CHEN, MARINA E. CHICUREL, LAURA DIKE, SUI HUANG, KYUNG-MI LEE, ANDREW MANIOTIS, ROBERT MANNIX, HELEN McNAMEE, CHRISTIAN J. MEYER, KEIJI NARUSE, KEVIN KIT PARKER, GEORGE PLOPPER, THOMAS POLTE, NING WANG, LI YAN, and DONALD E. INGBER

1. Introduction

For the past twenty years, our group has explored the possibility that cells and tissues use a form of architecture, known as 'tensegrity', to control their shape and to transduce mechanical signals into changes in biochemistry and gene expression (1–5). The importance of the tensegrity paradigm is that it predicts that the form and function of living cells are controlled through changes in mechanical interactions between cells and their underlying extracellular matrix (ECM) adhesions that, in turn, alter cytoskeletal and nuclear structure inside the cell (1–6).

Tensegrity structures gain their stability from continuous tension and local compression, much like a tent fabric stiffened by internal tent poles and external pegs (5). In contrast to conventional engineering models, which viewed the cell as a viscous cytosol surrounded by an elastic membrane, the tensegrity model assumes that the cell is a discrete (porous) mechanical network that requires prestress (internal tension) to fully stabilize itself. This model recognizes that the molecular elements of the cell are dynamic. However, it predicts that, at any instant in time, the entire cell will behave as if it were 'hard-wired' by a continuous series of molecular struts, cables, and ropes that stretch from specific adhesion receptors on the cell surface to physically couple to discrete contacts on the surface of the nucleus and from there to the chromatin and genes within (2–4, 7). In this type of structure, external mechanical signals would not be transmitted equally across all points on the cell surface, rather mechanical stresses should be preferentially transferred across specific transmembrane receptors that physically link the cytoskeleton to the ECM or to junctions on other cells (2, 6). Furthermore,

changes in the balance of forces transmitted through the cytoskeletal network should result in short- and long-range changes in molecular arrangements in the cytoskeleton and nucleus as well as associated alterations in thermodynamic and kinetic parameters that may influence cellular biochemistry (2, 4, 6). The tensegrity model, therefore, led to many testable predictions relating to how cells structure themselves as well as how they sense and respond to external mechanical signals.

Since this theory was first published, we have set out to systematically test these predictions. Because of the key roles of cell microarchitecture and mechanical forces in this model, this required that we develop entirely new experimental techniques that would allow us to control cell deformation independently of cell binding to growth factors or ECM as well as methods for applying controlled mechanical stresses to specific cell surface receptors. In this chapter, we describe these methods and briefly review new insights into cytoskeletal signalling and cell regulation that have emerged from these studies.

2. Application of techniques

2.1 Control of cell shape by varying extracellular matrix density

One of the fundamental predictions of the tensegrity model is that cell form and function are determined through *mechanical* interactions with the cell's ECM adhesions. The corollary to this is that cell shape, mechanics, and function should change if cell–ECM binding interactions are varied so as to prevent or promote cell distortion. Indeed, in early studies, we were able to show that the growth and differentiation of specialized cells (e.g. capillary endothelial cells, primary hepatocytes) can be controlled by altering the ability of the ECM substrate to resist cell tractional forces (8–10).

This was accomplished by varying the density of purified ECM molecules, such as fibronectin (FN), coated on otherwise non-adhesive, bacteriological plastic dishes, as described in *Protocol 1*. In these studies, the cells had to be cultured in serum-free medium to focus on effects of varying cell–ECM binding interactions, independently of exogenous matrix proteins that are found in high concentrations in serum (e.g. FN, vitronectin). When cells are plated on these dishes, cell spreading and growth increase in parallel as the ECM coating density is raised (8–10) (*Figure 1*). When spreading is restricted and growth suppressed, differentiation (e.g. tube formation by capillary cells, secretion of liver-specific proteins by hepatocytes) is concomitantly turned on (9, 10). This system has also been used to demonstrate shape-dependent control of cell contractility and mechanics in vascular smooth muscle cells (11). We are now using this as a model to analyse how changes in cell binding to ECM and concomitant alterations in cell shape modulate the intracellular

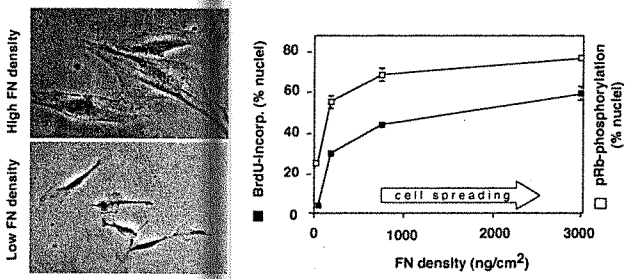

Figure 1. Modulation of cell shape. (*Left*) Phase-contrast view of human capillary endothelial cells plated on bacteriological dishes coated with high (*top*) and low (*bottom*) FN density. (*Right*) Cells plated on progressively higher FN density exhibit an increase in pRb phosphorylation and S phase entry as measured by nuclear BrdU incorporation. pRb phosphorylation was measured using *in situ* assay (12).

signalling cascade that controls this contractile response as well as cell cycle progression.

Protocol 1. Control of cell shape and function by varying ECM coating density

Equipment and reagents

- Bacteriological Petri dishes (Falcon Labware)
- 96-well plates (Immunolon II, Dynatech)
- Confluent cell monolayers
- Culture medium
- Lyophilized FN (Collaborative Biomedical Products, or Organon Teknika-Cappel, or Calbiochem)
- Carbonate buffer pH 9.4
- PBS
- 1% bovine serum albumin (BSA; Fraction V, Sigma)
- Trypsin-EDTA
- Serum-free media

Method

1. Two days prior to experiments, re-feed confluent cell monolayers with conventional culture medium containing low (0.5–1%) serum and no growth supplements in order to induce the cells to enter quiescence. Note: this may be difficult with transformed cells or certain cell lines. We have found that lovastatin provides an even more efficient method to synchronize cells in early G1 (12).
2. At least one day prior to experiment, resuspend purified ECM component, such as lyophilized FN in sterile distilled water (final concentration of 5 μg/ml) and store at 4 °C. Allow 30–60 min for material to go into solution; do not pipette, agitate, or swirl. Note: similar results

Protocol 1. *Continued*

have been obtained with FN from multiple commercial sources. Store aliquots of lyophilized ECM molecules at –70°C.

3. Dilute FN in carbonate buffer pH 9.4 to a final concentration that will add the required FN per well or dish in the following coating volumes: 100 μl/well in 96-well plates; 500 μl/24 mm dish, 5 ml/60 mm dish, 20 ml/100 mm dish, 30 ml/150 mm dish.
4. Incubate dishes overnight at 4°C. Dishes can be stored for longer times in the cold prior to use. Cover tightly with Parafilm to minimize evaporation.
5. On the day of experiment, aspirate coating solution, wash twice with PBS, once with basal medium, and then block non-specific binding sites by incubating dishes in medium containing 1% BSA at 37°C for at least 30 min.
6. While ECM-coated plates are sitting in medium containing 1% BSA, dissociate quiescent cell monolayers by brief exposure to trypsin-EDTA, collect by centrifugation, wash in medium containing 1% BSA to neutralize the trypsin, and plate cells on ECM-coated dishes in chemically-defined, serum-free medium. Note: use of serum to stop the trypsin will interfere with ECM-dependent control of cell shape and function; soybean trypsin inhibitor can also be added to ensure complete trypsin inactivation.
7. If the primary focus is on ECM-dependent control of cell shape and function, plate cells at a low density to minimize cell–cell contact formation in chemically-defined, serum-free medium containing 1% BSA. The exact composition of the medium will be dictated by the cell of choice. In certain cell types, such as capillary endothelial cells, higher plating densities are utilized when studies focus on control of ECM-dependent modulation of multicellular differentiation (e.g. capillary tube formation) (9).

2.2 Analysis of focal adhesion formation and integrin signalling

The results obtained with cells cultured on varying ECM densities demonstrated close coupling between cell spreading and growth (8–10), as demonstrated in past studies using other model systems (13). However, increasing the FN coating density does more than promote cell spreading, it also induces local clustering of cell surface ECM receptors, called integrins (14, 15). For this reason, it was necessary to develop methods to dissect out the biological effects induced by integrin clustering, independent of any associated cell shape change. We accomplished this by allowing round cells plated on a low FN density or suspended spherical cells to bind to small microbeads (4.5 μm

diameter) coated with a high density of FN, synthetic RGD-containing peptides, or specific anti-integrin antibodies (*Protocol 2*). Under these conditions, we could demonstrate that cells formed focal adhesion complexes (FACs) containing clustered integrins, talin, and vinculin, directly at the site of bead binding within 5–15 minutes after stimulation (16). In contrast, beads coated with a control ligand, acetylated-low density lipoprotein (AcLDL), bound to cell surfaces via transmembrane metabolic (scavenger) receptors but did not induce recruitment of any of these FAC proteins.

The rapid and synchronous induction of FAC formation obtained with this bead technique permitted an analysis of integrin signalling not possible with conventional methods. For example, we extended this work by using immunofluorescence microscopy to demonstrate that many signal transducing molecules that are turned on in response to binding to growth factor receptors as well as integrins (e.g. $pp60^{c\text{-}src}$, $pp125^{FAK}$, phosphatidylinositol-3-kinase, phospholipase C-γ, Na^+/H^+ antiporter, protein tyrosine phosphorylation) were also recruited to the cytoskeletal framework of the FAC in an integrin-specific manner and at similar times (17) (*Figure 2*). Finally, we took advantage of the fact that the beads we used were paramagnetic to develop a means to physically isolate these FACs away from the cell and remaining cytoskeleton (16, 17) (*Figure 3*; also see *Protocol 3*). Western blot analysis confirmed that FACs isolated using RGD-beads were enriched for $pp60^{c\text{-}src}$, $pp125^{FAK}$, phospholipase C-γ, and the Na^+/H^+ antiporter when compared with intact cytoskeleton or basal cell surface preparations that retained lipid bilayer. Isolated FACs were also greatly enriched for the high affinity fibroblast growth factor receptor. Most importantly, isolated FACs continued

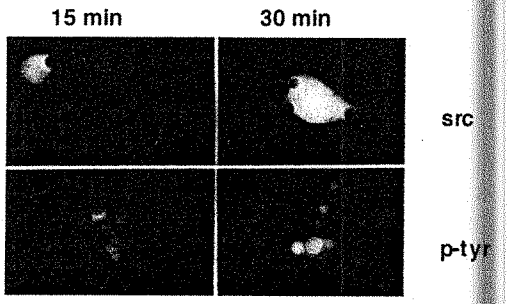

Figure 2. Recruitment of signalling molecules to the FAC in response to cell binding to FN-coated microbeads for 15 min (*left*) and 30 min (*right*). Positive immunostaining for src- and tyrosine-phosphorylated proteins is concentrated in a crescent-like pattern along the cell–bead interface.

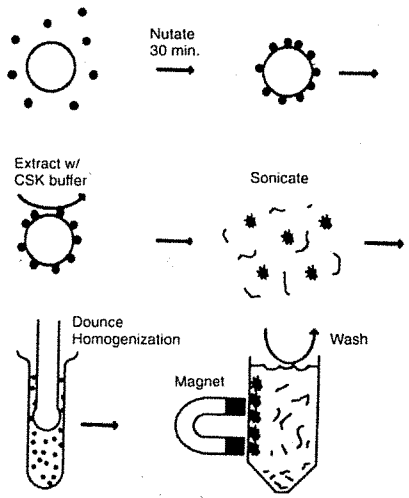

Figure 3. FAC isolation. Cells bound to RGD-coated beads were magnetically pelleted, extracted in CSK buffer, sonicated, and homogenized to remove nuclei and structures not intimately associated with the beads.

to exhibit multiple chemical signalling activities *in vitro*, including protein tyrosine kinase activities ($pp60^{c\text{-}src}$ and $pp125^{FAK}$) as well as the ability to undergo multiple sequential steps in the inositol lipid synthesis cascade (17, 18). This work, in combination with similar work from other laboratories (19), led to the realization that the FAC represents a major site for signal integration between growth factor and integrin pathways at the cell surface.

Protocol 2. Rapid induction of focal adhesion formation

Equipment and reagents

- Glass coverslips or slides (LabTek 8-well; Nalge NUNC International)
- Serum-free, chemically-defined medium
- Tosyl-activated magnetic microbeads (4.5 μm diameter; Dynal Inc.)
- 0.1 M carbonate buffer pH 9.4
- PBS
- 0.1% BSA
- Cytoskeleton stabilizing buffer (CSK–TX): 50 mM NaCl, 150 mM sucrose, 3 mM $MgCl_2$, 20 μg/ml aprotinin, 1 μg/ml leupeptin, 1 μg/ml pepstatin, 1 mM phenylmethylsulfonyl fluoride, 10 mM piperazine-*N*,*N*′-bis(2-ethanesulfonic acid) pH 6.8
- Triton X-100
- 4% paraformaldehyde

Method

1. Culture cells in serum-free, chemically-defined medium on glass coverslips or slides coated with a low FN density (e.g. 25–50 ng/cm²) to hold cells in a round form and prevent spreading, using *Protocol 1*. This coating concentration may vary between different cell types and should be determined empirically.
2. Coat tosyl-activated magnetic microbeads (4.5 μm diameter) with ECM molecule, synthetic RGD peptide (Peptide 2000), specific antibodies, or control ligands, such as AcLDL (Biomedical Technologies Inc.) at 50 μg/ml in 0.1 M carbonate buffer pH 9.4 for 24 h at 4°C (15, 16). Coated beads are washed twice in PBS, incubated in medium containing 1% BSA for at least 30 min, and then stored at 4°C in PBS. Note: microbeads from Dynal or other suppliers that are pre-coated with secondary antibodies or other cross-linking agents may be used in a similar manner.
3. Add coated microbeads to cells (20 beads/cell) and allow to incubate for 5–30 min at 37°C.
4. To identify cytoskeletal-associated FAC proteins, incubate cells for 1 min in ice-cold cytoskeleton stabilizing buffer (CSK–TX) which maintains the integrity of the cytoskeleton (20). Incubate for 1 min in the same buffer supplemented with 0.5% Triton X-100 (CSK+TX) to remove membranes and soluble cytoplasmic components. Note: removal of soluble cytoplasmic contents also greatly increases the signal-to-noise ratio of FAC protein staining and may be advantageous for any study that focuses on morphological analysis of the FAC.
5. Fix detergent-extracted cells in 4% paraformaldehyde/PBS, wash with PBS, and incubate with primary antibodies diluted in 0.2% Triton X-100/0.1% BSA in PBS. Visualize primary antibodies using the appropriate affinity-purified anti-IgGFc antibodies conjugated to fluorescein or rhodamine (Organon Teknika-Cappel).

Protocol 3. Isolation of focal adhesion complexes

Equipment and reagents

- See *Protocols 1* and *2*
- Polypropylene tubes (Costar)
- 15 ml conical tubes (Falcon)
- Rotator (Nutator)
- Side pull magnetic separation unit (Advanced Magnetics)
- XL 2005 cell disruptor (Heat Systems)
- Dounce homogenizer (Wheaton)
- 1% BSA/DMEM
- CSK–TX and CSK+TX buffer (see *Protocol 2*)
- RIPA buffer: 1% Triton X-100, 1% deoxycholate, 0.1% SDS, 150 mM NaCl, 50 mM Tris pH 7.2, 0.1 mM AEBSF

Protocol 3. *Continued*

Method

1. Disperse quiescent cells with trypsin-EDTA as described in *Protocol 1*, wash with 1% BSA/DMEM, and place cells in polypropylene tubes.
2. Suspend approx. 10^6 cells/ml in defined medium without growth factors, add an equal volume of medium containing RGD-coated magnetic microbeads (2×10^7 beads/ml; coated as in *Protocol 2*), and place on a rotator for 30 min at 37 °C. RGD-coated beads are utilized because they exhibit less non-specific clumping in suspension than FN-beads, and thus allow greater binding efficiency. However, similar results have been obtained with FN-coated beads.
3. Use a side pull magnetic separation unit to collect microbeads and bound cells. This and all subsequent procedures are carried out at 4 °C.
4. Resuspend cell/bead pellet in ice-cold CSK–TX buffer and transfer these to 15 ml conical tubes.
5. Re-pellet using magnetic separator. Resuspend bead pellets in cold CSK+TX buffer (with detergent), incubate on ice for 5 min, sonicate for 10 sec (output setting, 4; output power, 10%), and homogenize (20 strokes) in a (100 μm) Dounce homogenizer.
6. Pellet microbeads magnetically and wash five times with 10 ml CSK+TX buffer. RIPA buffer is used to remove protein from beads for biochemical analysis.

2.3 Geometric control of cell shape and function

This finding that integrin clustering alone is sufficient to activate internal signal transduction pathways that can influence cell behaviour complicated the cell shape story. However, the cells that bound to these beads which induced integrin clustering and early signalling events, including expression of immediate early growth response genes (21), never entered S phase (8). Thus, we then set out to make cell shape or distortion an independent variable. In other words, we attempted to devise a system in which cells could bind to optimal densities of ECM and soluble growth factors, but yet could be restricted in their spreading by purely physical means.

To control cell deformation in this manner, we adapted a soft lithography-based micropatterning technique that was originally developed in Dr George Whitesides' laboratory at Harvard as an alternative manufacturing approach for the microchip industry (22, 23). This method allowed us to create ECM-coated adhesive islands with defined shape, size, and position on the micron scale that were separated by non-adhesive, polyethylene glycol (PEG)-coated boundary regions that do not support protein adsorption and hence, prevent cell adhesion. When cells are plated on these substrates they adhere and

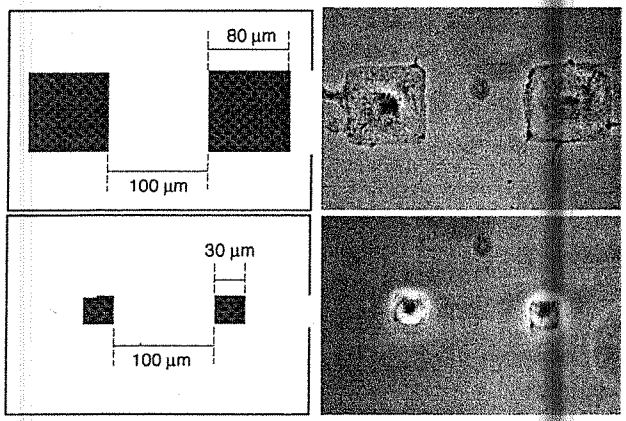

Figure 4. Control of human capillary endothelial cell shape using micropatterned substrates. Phase-contrast view (*right*) of CE cells plated on patterns containing FN-coated square islands 80 μm and 30 μm wide, respectively. The design of the pattern geometry is shown in the left panels, with the shaded area indicating the protein-adsorbing areas.

change their shape to fit the size and form of their container (i.e. of the patterned adhesive island) (24, 25) (*Figure 4*).

Methods for generating micropatterned substrates are described in *Protocols 4–8*. In brief, it involves a single photolithography step to generate a master etched pattern in silicon using a computer program commonly used for integrated circuit designs (23) (*Figure 5*). An elastomer (polydimethylsiloxane; PDMS) is then poured over the surface of this master and polymerized to form a 'rubber stamp' that retains the precise surface features of the micropattern down to less than 1 μm resolution. The outward facing features of the stamp are coated with a chemical 'ink' composed of alkanethiols. When the inked stamp is brought into contact with a gold-coated surface, the alkanethiols adhere tightly to the gold (Au) and self-assemble to form a space-filling monolayer that precisely fills the island form. A solution containing the same alkanethiol conjugated on its tail to a PEG blocking group is then poured over the slide surface. These alkanethiols self-assemble to fill all the spaces between the islands, creating a fully chemically-defined surface monolayer. However, because of the PEG blocking groups, ECM molecules will only adsorb to the surfaces of the islands when added in solution. This results in fabrication of highly adhesive, ECM-coated islands of defined shape, size, and position surrounded by non-adhesive, PEG-coated

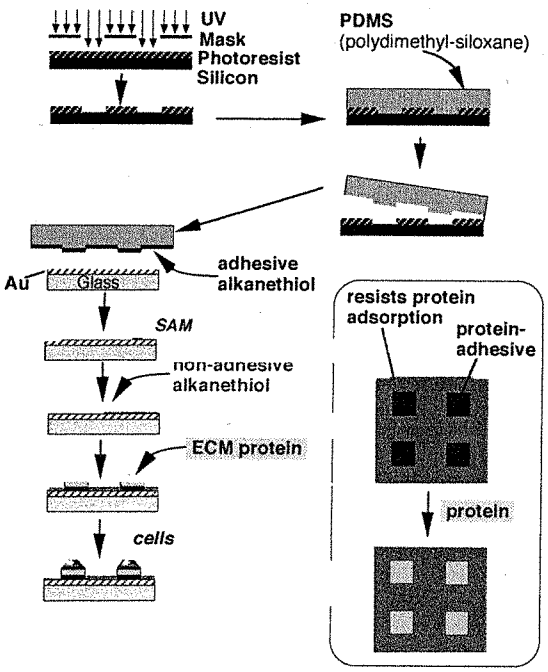

Figure 5. Schematic representation of the fabrication procedure for creating micropatterned substrates using microcontact printing. See text for details.

barrier regions. When cells are plated on these substrates they only adhere to the islands, spreading until they reach the surrounding non-adhesive boundary. By changing the size of the island, cells can be held in fully spread, moderately spread, or fully retracted form; by changing island form, cell shape can be controlled as well.

Using this micropatterning approach, we showed that capillary endothelial cells can be switched between growth, differentiation, and apoptosis programs simply by varying cell geometry (25, 26). For example, cells on large islands (50 μm diameter) that promoted cell extension supported growth, whereas cells on small islands (10 μm diameter) that remained fully retracted underwent a suicide program. To explore this mechanism, we allowed single cells to

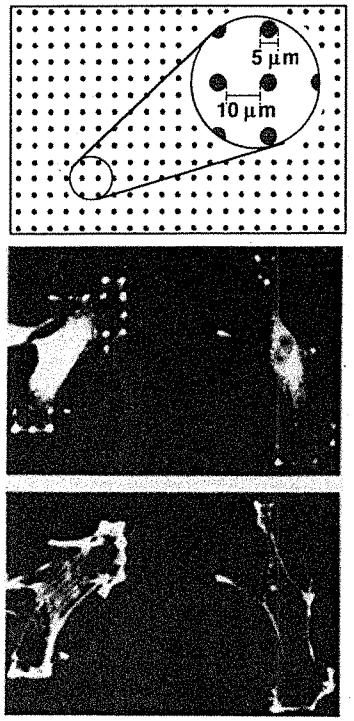

Figure 6. Micropatterns of 5 μm circles coated with fibronectin separated by 10 μm non-adhesive spaces (*top*), and immunofluorescence micrographs of adherent CE cells stained with anti-vinculin antibody (*middle*), and with FITC phalloidin (*bottom*) to visualize FACs and actin filaments, respectively.

spread across multiple, closely spaced, smaller adhesive islands that were the size of individual focal adhesions (3–5 μm diameter). Though the total area of these tiny islands was smaller than a single small (10 μm diameter) island, cells adherent to these patterned substrates spread as well as on a large island, stretching from island to island across non-adhesive areas (*Figure 6*). By increasing the spacing between islands, cell spreading could be increased by a

factor of ten without altering the total cell–ECM contact area. These observations revealed that cell shape—the degree to which the cell physically extends or retracts—governs whether cells grow or die (24). Most recently, using the same approach, we found that the motility of cells constrained on square adhesive islands is also controlled geometrically. Lamellipodia preferentially extend from the corners of these cells when stimulated with motility factors.

We are also using this micropatterning technique to expedite detection of focal adhesion-associated antigens in cells. Focal adhesion proteins commonly appear as small, spear-like streaks at the base of the cell when analysed by immunofluorescence microscopy. However, this is a highly subjective method and definitive characterization of a positively stained structure requires additional techniques, such as electron microscopy or interference reflection microscopy. By using substrates containing multiple focal adhesion-sized adhesive islands oriented in a regular pattern, we have overcome this limitation. Positive staining on these tiny islands represents antigens that are definitively concentrated in regions of cell anchorage to ECM and, hence, in focal adhesions. We are using this technique as a screening method, in conjunction with monoclonal antibody generation methods, to identify antibodies to novel focal adhesion proteins that may have structural or signalling roles relevant for cellular regulation.

Protocol 4. Generating a patterned silicon master using photolithography

Equipment and reagents

- Mask aligner (Karl Suss model)
- Silicon wafers
- Microscope
- Desiccator
- Trichloroethylene
- Acetone
- Methanol
- Hexamethyldisilazane (Shipley)
- 1813 positive photoresist (Shipley)
- (Tridecafluoro-1,1,2,2,-tetrahydro-octy)-1-trichlorosilane (United Chemical Technologies)

Method

1. Clean silicon wafers in a clean room (preferably Class A) by sonicating for 5 min successively in trichloroethylene, acetone, and methanol.
2. Heat wafers at 180°C for 10 min to dry thoroughly.
3. Spin coat (1500 g for 40 sec) the wafers with approx. 1–2 μm hexamethyldisilazane followed by a 1.3 μm thick layer of Shipley 1813 positive photoresist (1500 g for 40 sec).
4. Bake the resist at 105°C for 3.5 min.
5. Expose the wafer on a mask aligner through a photomask with features etched in chrome deposited on quartz (Advance Reproductions Corp.) for 5.5 sec at 10 mW/cm^2. The patterns on the photomask are normally created on a glass plate coated with photosensitive emulsion using a pattern generator. The final film is made by contact printing of the emulsion plate onto the chromium-coated quartz plate.
6. Develop the features by immersing in Shipley 351 for 45 sec, then rinse with distilled water, and dry with a stream of nitrogen. The proper development of the features should be checked under a microscope using a red filter in front of the light source to avoid unwanted exposure of the photoresist.
7. Place the wafers in a desiccator under vacuum for 2 h. Use a vial containing 1–2 ml (tridecafluoro-1,1,2,2-tetrahydro-octy)-1-trichlorosilane that reacts with the silicon areas not covered by the photoresist and makes them hydrophobic. Rinse only with water and avoid all contact with organic solvents.

Protocol 5. Moulding elastomeric microstamps

Equipment and reagents

- Petri dishes
- Razor blade
- Polydimethylsiloxane (PDMS) (Sylgard 184, Dow Chemical Co.)

Method

1. Polydimethylsiloxane (PDMS) pre-polymer is made by mixing ten parts of monomer Silicone Elastomer-184 and one part of initiator Silicone Elastomer Curing Agent-184 thoroughly in a plastic container and degassing it under vacuum for approx. 1 h until air bubbles no longer rise to the top.
2. Pour the pre-polymer in a Petri dish that contains the patterned silicon wafer, and cure for at least 2 h at 60°C. Often small air bubbles form in the PDMS after it is poured on the master stamp. Cover the dish and gently tap it to allow the bubbles to diffuse out of the pre-polymer. Typically, stamps are 0.5–1 cm tall.
3. Peel the PDMS from the wafer and cut the stamps to the desired size with a razor blade. During curing, a layer of PDMS forms underneath the wafer and holds it to the dish. Invert the dish and gently press on the reverse side until the cured PDMS dewets from the surface of the dish. Invert the dish and use a dull edge to trace the contour of the PDMS so as to lift it off the dish. Often the PDMS remains attached to the wafer. Carefully cut the layer of PDMS found under the wafer and gently peel the two surfaces away from each other.

Protocol 6. Metal coating of glass substrates

Equipment and reagents

- Microscope slides (Fisher, No. 2)
- Electron beam evaporator
- Titanium (Aldrich, 99.99% purity)
- Gold (Materials Research Corporation, 99.99% purity)

Method

1. Load microscope slides on a rotating carousel in an electron beam evaporator (most of these are home-built).
2. Perform evaporation at pressure $< 1 \times 10^{-6}$ Torr. Occasionally, during the evaporation of titanium, the pressure increases above 1×10^{-6} Torr, but decreases after allowing the chamber to stabilize for approx. 2 min. Note: a sputter coat system also may be used to prepare these coatings. However, we recommend using an evaporator to coat the substrates because most sputter coaters are single source and, thus, they are impractical for coating two different metals (Ti and Au) on a single substrate. In addition, sputtering gives less homogeneous films that require an additional annealing step. Sputtering systems also generally produce films with higher quantities of metal oxides and other impurities that could interfere with the generation of the self-assembled monolayer (SAM) surface.
3. Allow the metals to reach evaporation rates of 1 Å/sec.
4. Allow 400–500 Å of each metal to evaporate before opening the shutters and exposing the glass slides to 15 Å of titanium (99.99% purity) followed by 115 Å of gold (99.99% purity).

Notes on storage: typically, gold-coated substrates become 'mottled' after four to five weeks and are no longer deemed suitable for experiments; streaks with heterogeneous transparency develop (they are obvious to the naked eye). This may be caused by rearrangements in the thickness of the gold layer related to impurities present on the glass before evaporation of the gold. Gold substrates that are stamped immediately after evaporation are generally more stable over time (approximately three months), perhaps because the SAM acts as a resist against impurities.

Protocol 7. Stamping micropatterned adhesive substrates

Equipment and reagents

- Q-tips
- Forceps
- Pasteur pipette
- Gold-coated substrate
- PDMS stamp
- 2 mM solution of hexadecanethiol ($HS(CH_2)_{15}CH_3$) (Aldrich) in ethanol
- 2 mM PEG-terminated alkanethiol: tri(ethylene glycol)$HS(CH_2)_{11}(OCH_2CH_2)_3OH$ (synthesized at Dr G. Whitesides' laboratory)

Method

1. Lay metal-coated substrate on clean flat surface, with gold facing upward. Take care not to scratch the surface with sharp forceps, or to place the substrate upside down. If there is dust visible on the substrate, blow gently with pressurized air or nitrogen.
2. Rinse the PDMS stamp with ethanol and remove the ethanol vigorously with a stream of pressurized air or nitrogen for at least 10 sec. If any dust remains on the stamp, repeat this procedure.
3. Dip a Q-tip into a 2 mM solution of hexadecanethiol in ethanol and gently paint a layer of the solution onto the PDMS stamp. Use a stream of air or nitrogen to gently evaporate the ethanol off the stamp.
4. Gently place the stamp face down onto the gold-coated substrate and allow it to adhere; this step may require gentle pressure. Let the fully adhered stamp remain on the substrate for at least 10 sec. Observe the light reflected from the micropatterned substrate at an angle to ensure that the stamp has fully adhered to the substrate. A pink colour will ensure that full adhesion has occurred. Both under-stamping and over-stamping results in a loss of this interference pattern. Make sure that no patches of non-adhesion remain.
5. Use forceps to gently peel away the stamp from the substrate, making sure not to move the stamp against the substrate or to let the stamp re-adhere to the substrate.
6. Return to step 2 to continue stamping more substrates. After all substrates are stamped, proceed with step 7.
7. Use a Pasteur pipette to deliver an ethanol solution containing 2 mM PEG-terminated alkanethiol [tri(ethylene glycol)$HS(CH_2)_{11}(OCH_2CH_2)_3OH$] dropwise onto each substrate until the liquid covers it entirely. This usually requires approx. 0.5–1 ml per square inch of substrate. Incubate with the PEG-alkanethiol for 30 min to fill in the remaining bare regions of gold and complete the self-assembled monolayer surface coating. Note: always stamp the hexadecanethiol, rather than the PEG-alkanethiol. Stamping the PEG-alkanethiol results in less efficient pattern transfer, incomplete formation of the self-assembled monolayer, and non-specific adsorption of proteins in the 'non-adhesive' PEG-coated barrier regions.
8. With forceps—cleaned with ethanol and blown dry—grasp the corner of the substrate and rinse with a stream of ethanol on both sides of the pattern for 20 sec. Place the substrate on a clean surface and rinse the forceps with ethanol. Grasp the substrate again in a different location and rinse with ethanol to wash the area previously masked by the forceps.

Protocol 8. *Continued*

9. Blow off ethanol from the substrate with pressurized air or nitrogen.
10. Place the stamped substrates into containers, taking care not to allow the patterned surface to rub against any coarse surfaces. Store under nitrogen gas in a cool, dark location. Place the containers in a Ziplock bag filled with nitrogen.

Notes on storage: typically, alkanethiols kept in ethanolic solutions for more than three months become oxidized and form significant amounts of disulfides. Disulfides of PEG are detected by TLC as spots with an R_f of approximately 0.15, while the thiol has an R_f of 0.25 using CH_2Cl_2:CH_3OH (98:2) as the eluent. By NMR, disulfides can be distinguished from alkanethiols by the presence of a triplet of peaks (from the methylene group adjacent to the sulfur atom) at approximately 2.6 p.p.m. instead of a quartet at 2.5 p.p.m. Although disulfides are known to form SAMs with interfacial properties similar to those formed with alkanethiols, their assembly is 75 times slower.

Protocol 8. Culturing cells on micropatterned substrates

Equipment and reagents

- Petri dishes
- Microscope
- PBS
- ECM protein (25 μg/ml)
- 1% BSA dissolved in PBS
- Trypsin-EDTA
- 1% BSA/DMEM
- Serum-free media

Method

1. Prepare a solution of phosphate-buffered saline (PBS) containing the ECM protein (25 μg/ml) to be coated on the adhesive islands.
2. Place a small droplet (0.25 ml) of ECM solution onto a bacteriological Petri dish or another disposable hydrophobic surface that is non-adhesive for cells in the absence of serum. Typically, 0.25 ml of solution per square inch of substrate is sufficient. Float each substrate, with patterned side face-down, on the drops. Let sit for 2 h at room temperature.
3. After 2 h, add a large amount (5–15 ml) of 1% BSA dissolved in PBS directly to the dish in order to dilute the ECM protein solution and block further coating. Remove the substrates, flip the slide so that micropattern side is facing-up, and place directly into serum-free medium containing 1% BSA. Note: when adding the BSA/PBS solution, the slides can sink onto the dish and adhere to it; since the substrates face the bottom of the dish, the pattern may be damaged. To avoid this, gently add the BSA solution around the edges of the substrate so that the slides remain afloat.
4. Dissociate quiescent cell monolayers by brief exposure to trypsin-EDTA, wash, and resuspend in 1% BSA/DMEM, as described in *Protocol 1*. Remove one-half volume of 1% BSA/DMEM from Petri dishes containing the micropatterned substrates and replace with an equal volume of medium containing cells at a low plating density (e.g. 7500 cells/cm^2) plus any required medium supplements at twice the concentration. Note: if serum-containing medium must be utilized, initially plate cells for at least 1 h in serum-free medium (this may only be necessary for certain cell types). Subsequent medium changes should minimize drying, which can non-specifically adsorb medium proteins onto the substrate and thus, compromise shape control. We commonly remove 75–90% of the old medium and replace it with new at each refeeding rather than remove all fluid during these medium changes. Note: a low cell plating density is utilized to optimize plating of single cells on individual islands and because the actual surface area available for cell adhesion on the patterned slides is a fraction of that of a regular culture dish. The cell plating densities and medium conditions will vary between different cell types and thus, should be determined empirically.
5. Visualize cells by any standard microscopic technique when micropatterning is performed on glass slides. Immunofluorescence staining of cytoskeletal and FAC components may be performed as described in *Protocol 2*.

2.4 Analysis of transmembrane mechanical signalling

The tensegrity model predicts that ECM regulates cell shape and function based on its ability to balance cytoskeletal tension that is transmitted across discrete transmembrane adhesion receptors on the cell surface. To analyse the molecular mechanism by which cells transfer external mechanical signals across the cell surface and to the cytoskeleton, we developed a magnetic twisting device (magnetic cytometry system) in which controlled mechanical stresses can be applied directly to specific subclasses of receptors on the surface of living cells (27, 28). In this technique, cultured cells are allowed to bind to small ferromagnetic beads coated with specific receptor ligands, as described in *Protocol 2*. Shear stress (torque) is applied to the membrane receptor-bound ferromagnetic microbeads by magnetically twisting the beads. This is accomplished by first magnetizing the beads by applying a very brief, but strong, homogeneous magnetic field in the horizontal direction. Then a weaker, but sustained magnetic field is applied in the vertical direction. This does not remagnetize the beads; instead, the beads realign along the new

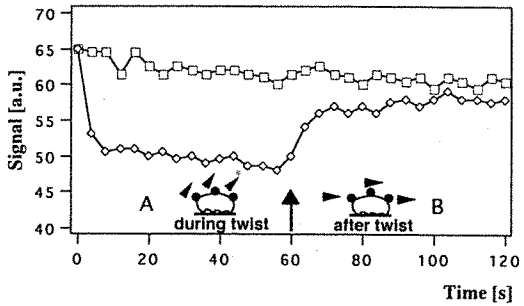

Figure 7. Data obtained using magnetic twisting cytometry showing the magnetic signal in the absence (squares) and presence (diamonds) of the twisting field. Application of a constant twisting stress (40 Gauss) for 60 sec in the vertical direction results in an instantaneous decrease in the signal. The difference in signal (on/off) at 60 sec is used to calculate the apparent stiffness, *E*. The rate of recovery after 60 sec multiplied by *E* determines the apparent viscosity (see *Equation 1*).

applied field lines much like a compass needle. Thus, the cellular response to applied stress can be measured simultaneously by quantifying changes in the rate and degree of magnetic bead rotation (i.e. angular strain) using an in-line magnetometer (*Figure 7*). This method is described in *Protocol 9*. Note: ferromagnetic beads must be used in these studies because, in contrast to the paramagnetic beads we utilized in our FAC isolation procedure, these materials must maintain their magnetization when an applied magnetic field is removed.

The values of the material properties measured using this technique will vary depending on the cell surface receptor to which that force is applied. Thus, this method allows one to measure micromechanical behaviour of different molecular supporting frameworks in the cell. When force is applied through cell surface integrins, the resulting shear stress is transmitted through the cell, causing the intracellular cytoskeleton to deform without producing large scale changes in cell shape (27). Using this technique, we showed that integrin receptors efficiently mediate mechanical force transfer across the cell surface through the FAC and to the cytoskeleton in endothelial cells and vascular smooth muscle cells, although different receptor subtypes varied in their response (integrin $\beta1 > \alpha Vb3 > \alpha5 > \alpha2 > \alpha V$) (11, 27–33). Other adhesion receptors, such as cadherins and selectins, mediated mechanical force transfer to the cytoskeleton to a moderate degree, whereas transmembrane receptors not involved in adhesion, such as metabolic scavenger

receptors and histocompatibility antigens, displayed minimal mechanical coupling (27, 31, 34). In addition, we consistently found that the stiffness (i.e. the ratio of stress to strain) of the cytoskeleton increased in direct proportion to the applied stress and thus, that the cytoskeleton behaves as a tensionally-integrated or 'tensegrity' structure (27).

Additional support for this model came from the finding that the mechanical stiffness at the cytoskeleton depended directly on the level of pressure (pretension) in the cytoskeleton (11, 30, 35).

We recently showed that the same magnetic twisting method can be used to analyse mechanochemical signalling in living cells. For this application, the magnetometer is used to verify the level of applied mechanical twisting stresses rather than to record experimental data. Changes in cellular biochemistry are measured simultaneously using conventional biochemical and molecular biological techniques. For example, magnetically twisting beads bound to cell surface integrins in adherent endothelial cells were found to induce recruitment of total poly(A) mRNA and ribosomes to the focal adhesions that form at the site of bead binding, as detected using high resolution *in situ* hybridization and immunofluorescence microscopy (36). Recruitment of the protein translation machinery was shown to be integrin-specific and dependent on the level of applied mechanical stress. These data suggest that altering the balance of mechanical forces, specifically across integrins, changes the intracellular biochemistry and, in this case, induces the formation of a microcompartment at the focal adhesion specialized for protein synthesis. Again, these results add experimental support for the predictions made by the tensegrity model. We are now using this method of localized stress application in cells expressing GFP-labelled cytoskeletal proteins (e.g. actin, tubulin, vinculin) to analyse directly how the cytoskeleton bears and distributes mechanical loads.

Protocol 9. Magnetic twisting cytometry

Equipment and reagents

- Spherical ferromagnetic beads obtained commercially (4.5 μm diameter, CFM-40-10 carboxylated-ferromagnetic beads; Spherotech) or from independent laboratories (1.4 μm or 5.5 μm diameter beads; Dr W. Moller, Gauting, Germany)
- Magnetic twisting device
- In-line magnetometer
- 96-well Removawells (Immunolon II)
- 100 000 centipoise, PSAV100K (Petrarch Systems Inc.)

Method

When carboxylated-Spherotech beads are utilized, ligands are conjugated at 50 μg/ml using a carbodiimide (EDC; Sigma E-6383) reaction, as described by the supplier. The other beads are coated with adhesive ligands or antibodies at the same concentration, using methods described for paramagnetic Dynal microbeads in *Protocol 2*. Beads may also be

Protocol 9. *Continued*

obtained pre-coated with secondary antibodies (e.g. goat anti-mouse IgG Fc domain), to which can be added primary antibody in sterile PBS at 10–50 μg/ml (this concentration needs to be determined empirically for each antibody to ensure optimal binding). Store beads in sterile PBS at 4°C. Note: do not magnetically separate during washing steps because these beads will remain magnetized and thus, will be difficult to dissociate.

1. Plate cells (3×10^4/well) on FN-coated bacteriological plastic dishes (96-well Removawells) and culture for 6–10 h in chemically-defined medium before bead addition. The beads are quenched in chemically-defined medium containing 1% BSA for at least 30 min before being added to the cells.
2. Add approx. 1–10 beads/cell (this should be determined experimentally to obtain approx. 1–4 bound beads/cell) and incubate in chemically-defined medium containing 1% BSA for 15–30 min. At this time, the cells are washed in serum-free medium to remove unbound beads.
3. Place the individual well containing cultured cells and bound beads within a plastic vial, and then place it into the holder of the magnetic twisting device. Rotate at a constant rate (5 r.p.m.) to reduce ambient noise. The vial prevents the circulating water used for temperature control from getting into the culture well.
4. Apply a brief (10 μsec) but strong (1000 Gauss) magnetic pulse in the horizontal direction (parallel to the culture surface), using one pair of the magnetic coils of the device. After several seconds, apply a much weaker magnetic twisting field (0–40 Gauss) in the vertical direction and twist the beads for 1 min. The vertical field can be altered to assess the effects of force duration and frequency as well as the form of the stress regimen (e.g. square wave versus sinusoidal).
5. Use an in-line magnetometer to detect changes in the magnitude of the bead magnetic vector in the horizontal direction. Note: the torque of the applied twisting field is proportional to the twisting field, bead magnetization, and the sine of the angle between the twisting field vector and the bead magnetization vector (27). In the absence of force transmission across the cell surface, the spherical beads turn in place by 90° into complete alignment with the twisting field, and the remaining field vector immediately drops to zero. In contrast, transmission of force to the cytoskeleton results in increased resistance to deformation and decreased bead rotation. Angular strain (bead rotation) is calculated as the arc cosine of the ratio of remanent field after 1 min twist to the field at time 0.

6. Determine the apparent stiffness (ratio of stress to strain) and viscosity using the following relation:

$$E = \frac{\sigma}{\phi} \quad \text{and} \quad \eta = E\tau \qquad [1]$$

where E is the apparent stiffness; σ is the effective stress; ϕ is the angular rotation of the microbead; η is the apparent viscosity; and τ is the time constant of recovery after stress release. In the absence of the applied twisting field, the magnetic signal exhibits only a small decrease or relaxation in signal that is due to thermal motion and membrane movement. However, when a constant twisting field (e.g. 30 Gauss) is applied in the vertical direction for 1 min, the magnetic signal of the beads decreases almost instantaneously (to zero when the beads are free in solution). By subtracting the relaxation signal from the control, the remanent field signal almost reaches a plateau after 1 min. This plateau value obtained 1 min after stress application (representing magnetic torque being balanced by the elastic component of the cell) is used to calculate the apparent stiffness of the cell according to the above relation (*Figure 7*).

7. Quantitate the energy stored elastically in the cell by turning off the twisting field for 1 min and measuring the extent of recovery of the bead magnetic signal. The difference in the signal that remains after 2 min relative to the remanent field signal is a readout of permanent deformation.
8. Calibrate the effective applied stress by placing microbeads in a standard solution of known viscosity (e.g. 100 000 centipoise, PSAV100K) (28, 29) and measuring angular strain. The effective stress equals:

$$\sigma = cH_a \frac{B_{twist}}{B_{relax}}\ ;\ \phi = \cos^{-1}\left(\frac{B_{twist}}{B_{relax}}\right) \qquad [2]$$

where c is a constant dependent on the magnetic property of the bead:

$$c = v \times 1/T$$

where v is the standard viscosity; $1/T$ is the slope of $tan\ (90° - \phi/2)$ versus time; H_a is the applied twisting field; B_{twist} is the remaining twisting signal at 60 sec; B_{relax} is the remanent relaxation signal at 60 sec. Note: it is assumed that the angular rotation of the bead is a direct readout of the angular strain of the cell.

For studies on mechanochemical transduction, controlled stresses are applied in a similar manner, and biochemical or morphological changes are measured inside the cells using conventional analytical techniques. For example, cells plated on small ECM-coated coverslips can be bound to magnetic beads, twisted, fixed, and then analysed using *in situ* hybridization or

immunofluorescence microscopy (36). It is also possible to use this technique to twist large numbers (millions) of suspended cells bound to magnetic beads in order to measure biochemical changes inside the cells (e.g. cAMP levels). Larger numbers (10–20) of beads bound per cell may be utilized for these studies.

2.5 Detection of long-range mechanical signal transfer

The tensegrity model of integrated cell shape control assumes that transmembrane ECM receptors, cytoskeletal filaments, and nuclear scaffolds are 'wired' together in such a way that mechanical stimuli can change the organization of molecular assemblies deep in the cytoplasm and nucleus. This is contrary to many existing models which view the cell as a viscous cytoplasm surrounded by an elastic membrane that bears most of the mechanical load. We recently developed a microsurgical approach to demonstrate that living cells and nuclei are indeed hard-wired such that a mechanical tug on cell surface receptors can immediately change the organization of molecular assemblies in the cytoplasm and nucleus (37). Specifically, when integrins were pulled by micromanipulating bound ECM-coated microbeads or micropipettes, cytoskeletal filaments reoriented, nuclei distorted, and nucleoli redistributed along the axis of the applied tension field. These effects were specific for integrins, independent of cortical membrane distortion, and mediated by direct linkages between the cytoskeleton and nucleus.

We extended these studies to analyse long-distance stress transfer and connectivity in the cytoskeleton and the nucleus, by using a very fine microneedle (0.5 μm diameter) to 'harpoon' the cytoplasm at precise distances from the nucleus and then rapidly pulling it away from the nucleus, toward the cell periphery (37). Cells remained viable during this procedure. We used digitized image analysis and real-time video microscopy to determine the position of multiple phase-dense structures within the cytoplasm and the nucleus (e.g. mitochondria, vacuoles, nucleoli, nuclear envelope) before and after pulling the micropipette away from the nucleus using the micromanipulator. By harpooning the cytoplasm with uncoated micropipettes and applying stresses directly to the cytoskeleton in cells treated with different cytoskeleton-modulating drugs, we were able to show that actin microfilaments mediated force transfer to the nucleus at low strain; however, tearing of the actin gel resulted in greater distortion (37). In contrast, intermediate filaments effectively mediated force transfer to the nucleus under both conditions, and cell tearing resulted when intermediate filaments were disrupted either by pharmacological means (37) or using genetic recombination (38). Finally, by placing the pipette tip closer to the nuclear border (2–4 μm) or within the nucleoplasm itself and then pulling away from the nuclear envelope, we could demonstrate the presence of discrete (localized) sites of mechanical stress transfer between the cytoplasm and nucleus as well as between the nucleoplasm and the nuclear envelope (37) (*Figure 8*).

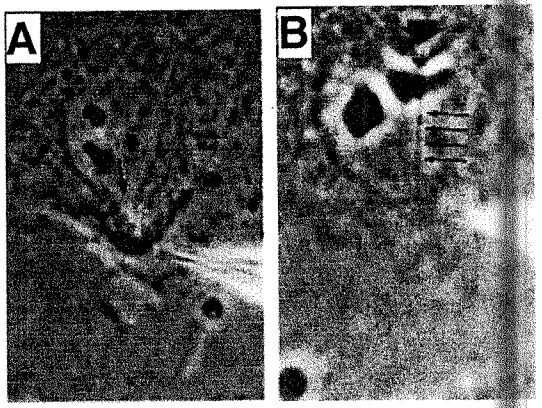

Figure 8. Demonstration of discrete connections between cytoskeletal and nuclear scaffolds. (A) A cell harpooned by a microneedle close to the nuclear border after stress application. The *arrow* indicates a local tongue-like protrusion of the nuclear envelope. (B) Invagination of the nuclear envelope in response to harpooning the nucleoplasm. Four small *arrows* indicate the tensed nucleoplasmic thread stretching from the pipette tip.

We also used the harpooning approach to estimate relative changes in mechanical stiffness of the cytoplasm and nucleus (37). The stiffness (E) of the cytoplasm and nucleus, as in any material, equals stress (s) (force/cross-sectional area) divided by strain (e) (change in length/initial length). The stiffness of the cytoplasm and nucleus cannot be determined directly using the harpooning technique, because only induced strains are measured. However, the ratio of stiffness in the cytoplasm (c) and nucleus (n) can be determined in the following manner (*Figure 9*). The ratio of nuclear to cytoplasmic stiffness (E_n/E_c) will equal the ratio of cytoplasmic to nuclear strain ($\varepsilon_c/\varepsilon_n$) measured in these regions when exposed to the same stress. If the cell responds isotropically and homogeneously to stresses applied over short (micrometre) distances, then the stress tensor (three-dimensional stress field) produced at any point will depend primarily on its location relative to the site of force application. Thus, the ratio of nuclear to cytoplasmic stiffness can be calculated by determining the ratio of induced strains measured in regions of the cytoplasm and nucleus when placed at the same distance from the micropipette (i.e. even if in different regions of the cell). We adapted the harpooning method to quantitate apparent Poisson's ratios as a measure of mechanical connectivity within the cytoplasm and nucleus of living cells.

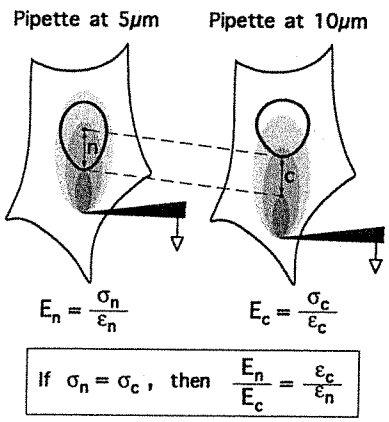

Figure 9. Schematic diagram demonstrating how relative changes in the mechanical stiffness of the cytoplasm and nucleus can be analysed in living cells.

Based on these studies, we found that intermediate filaments and actin filaments acted as molecular guy wires to mechanically stiffen the nucleus and anchor it in place, whereas microtubules acted to hold open the intermediate filament lattice and to stabilize the nucleus against lateral compression. Thus, these results added direct experimental support for our hypothesis that molecular connections between integrins, cytoskeletal filaments, and nuclear scaffolds may provide a discrete path for long-range mechanical signal transfer through cells as well as a mechanism for producing integrated changes in cell and nuclear structure in response to changes in ECM adhesivity or mechanics. Our methods for analysis of long-distance force transfer through the cytoskeleton as well as cytoplasmic and nuclear mechanics are presented in *Protocols 10* and *11*.

Protocol 10. Microsurgical analysis of long-range mechanical signalling

Equipment and reagents

- FN-coated glass coverslips
- Needles (Narishige)
- Pipette puller (Sutter)
- Manual micromanipulator (Leitz)
- Tosyl-activated microbeads (4.5 μm diameter; Dynal)
- Culture media

Method

1. Culture cells for 6–24 h in serum-free, chemically-defined medium containing 1% BSA on FN-coated glass coverslips. For studies involving force application to cell surface integrins, cells should be cultured on a suboptimal FN density (200–400 ng/cm^2) that promotes only a moderate degree of spreading, using the method in *Protocol 1*. Note: long-range distance transfer is difficult to visualize in well-spread cells on a high ECM density because these cells are too stiff, and most of the applied load is borne by their basal adhesions to the rigid ECM-coated substrate.
2. Pull needles with pipette puller and affix them to a manual micromanipulator. The micropipettes should be formed with tips approx. 0.5–1 μm wide along a length of 40–100 μm.
3. Add microbeads (4.5 μm diameter, tosyl-activated) coated with integrin ligands, as described in *Protocol 2*, to cells (1–4 beads/cell) for 10–15 min. Beads should be bound to cells at this time, but not internalized.
4. Wash cells with cell culture medium to remove unbound beads. Transfer the coverslip onto the lid of 35 mm Petri dish filled with DMEM, and place it in the heated chamber (Omega RTD 0.1 stage heating ring at 37 °C) on the stage of an inverted microscope.
5. Position the tip of the uncoated glass micropipette alongside the surface-bound beads using the micromanipulator. Rapidly pull the bead away from the cell (about 5–10 μm/sec), parallel to dish surface.
6. Measure nuclear distortion, movement of the nuclear border, and any other cellular response to stress (e.g. redistribution of phase-dense organelles, such as mitochondria, vacuoles, or secretory granules) in the direction of the applied tension field using inverted phase-contrast, fluorescence, Nomarski, or birefringence microscopy in conjunction with real-time computerized image analysis (we use Oncor *Image Analysis* software).

Protocol 11. Analysis of stress transfer through the cytoskeleton

Equipment and reagents

- Nocodazole (10 μg/ml; Sigma), acrylamide (5 mM; Bio-Rad), or cytochalasin D (0.1–1 μg/ml; Sigma)
- Glass micropipette (0.5 μm diameter)
- See *Protocol 10*

Method

1. To analyse force transfer between the cytoskeleton and nucleus, 'harpoon' the cytoplasm with an uncoated glass micropipette (0.5 μm

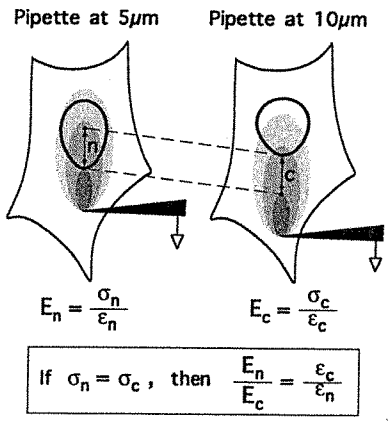

Figure 9. Schematic diagram demonstrating how relative changes in the mechanical stiffness of the cytoplasm and nucleus can be analysed in living cells.

Based on these studies, we found that intermediate filaments and actin filaments acted as molecular guy wires to mechanically stiffen the nucleus and anchor it in place, whereas microtubules acted to hold open the intermediate filament lattice and to stabilize the nucleus against lateral compression. Thus, these results added direct experimental support for our hypothesis that molecular connections between integrins, cytoskeletal filaments, and nuclear scaffolds may provide a discrete path for long-range mechanical signal transfer through cells as well as a mechanism for producing integrated changes in cell and nuclear structure in response to changes in ECM adhesivity or mechanics. Our methods for analysis of long-distance force transfer through the cytoskeleton as well as cytoplasmic and nuclear mechanics are presented in *Protocols 10* and *11*.

Protocol 10. Microsurgical analysis of long-range mechanical signalling

Equipment and reagents

- FN-coated glass coverslips
- Needles (Narishige)
- Pipette puller (Sutter)
- Manual micromanipulator (Leitz)
- Tosyl-activated microbeads (4.5 μm diameter; Dynal)
- Culture media

Method

1. Culture cells for 6–24 h in serum-free, chemically-defined medium containing 1% BSA on FN-coated glass coverslips. For studies involving force application to cell surface integrins, cells should be cultured on a suboptimal FN density (200–400 ng/cm^2) that promotes only a moderate degree of spreading, using the method in *Protocol 1*. Note: long-range distance transfer is difficult to visualize in well-spread cells on a high ECM density because these cells are too stiff, and most of the applied load is borne by their basal adhesions to the rigid ECM-coated substrate.
2. Pull needles with pipette puller and affix them to a manual micromanipulator. The micropipettes should be formed with tips approx. 0.5–1 μm wide along a length of 40–100 μm.
3. Add microbeads (4.5 μm diameter, tosyl-activated) coated with integrin ligands, as described in *Protocol 2*, to cells (1–4 beads/cell) for 10–15 min. Beads should be bound to cells at this time, but not internalized.
4. Wash cells with cell culture medium to remove unbound beads. Transfer the coverslip onto the lid of 35 mm Petri dish filled with DMEM, and place it in the heated chamber (Omega RTD 0.1 stage heating ring at 37 °C) on the stage of an inverted microscope.
5. Position the tip of the uncoated glass micropipette alongside the surface-bound beads using the micromanipulator. Rapidly pull the bead away from the cell (about 5–10 μm/sec), parallel to dish surface.
6. Measure nuclear distortion, movement of the nuclear border, and any other cellular response to stress (e.g. redistribution of phase-dense organelles, such as mitochondria, vacuoles, or secretory granules) in the direction of the applied tension field using inverted phase-contrast, fluorescence, Nomarski, or birefringence microscopy in conjunction with real-time computerized image analysis (we use Oncor *Image Analysis* software).

Protocol 11. Analysis of stress transfer through the cytoskeleton

Equipment and reagents

- Nocodazole (10 μg/ml; Sigma), acrylamide (5 mM; Bio-Rad), or cytochalasin D (0.1–1 μg/ml; Sigma)
- Glass micropipette (0.5 μm diameter)
- See *Protocol 10*

Method

1. To analyse force transfer between the cytoskeleton and nucleus, 'harpoon' the cytoplasm with an uncoated glass micropipette (0.5 μm

Protocol 11. *Continued*

diameter) 10 μm from the nuclear border and then pull the pipette away, first 10 μm and then 20 μm at a rate of 5–10 μm/sec (*Figure 8*).

2. Culture cells in the presence of nocodazole (10 μg/ml), acrylamide, (5 mM), or cytochalasin D (0.1–1 μg/ml) to disrupt or compromise microtubules, intermediate filaments, or microfilaments, respectively. Note: doses need to be adjusted for different cell types, and immunofluorescence staining should be carried out in parallel to ensure that the effects are specific and maximal.
3. Measure resultant changes in nuclear deformation induced by the 10 μm and 20 μm pulls simultaneously, using real-time video microscopy in conjunction with computerized image analysis, as described in *Protocol 10*.
4. Calculate nuclear strains in the direction of pull at 10 μm and 20 μm displacements. Nuclear movement is defined as displacement of the rear border of the nucleus in the direction of pull. Negative lateral nuclear strain (nuclear narrowing) is calculated by measuring changes in nuclear width perpendicular to the direction of pull.
5. To demonstrate direct connections between the cytoskeleton and nucleus, apply tension via a pipette placed closer to the nuclear border (2–4 μm). Note: if the cytoplasm pulls away from the nuclear border without deforming the nucleus or by causing it to narrow along its entire length (i.e. sausage-casing type effect), then the two structures are merely interposed with no connectivity. If stress application causes a small region of the nuclear envelope to protrude locally toward the pipette in the region of highest stress (*Figure 8*), then a direct connection must exist.
6. To demonstrate the presence of a distinct filamentous network within the nucleus, harpoon the nucleoplasm and pull inward. Local indentation of the nuclear border again indicates the presence of direct mechanical coupling at a localized site (*Figure 8*).

Protocol 12. Analysis of nuclear and cytoplasmic stiffness and connectivity

Equipment and reagents

- See *Protocols 10* and *11*

Method

1. To determine the ratio of nuclear to cytoplasmic stiffness, calculate strains in the direction of pull within regions of the nucleus and

cytoplasm located at the same distance from a pipette that is pulled 10 μm toward the cell periphery. This is accomplished by placing the pipette 5 μm or 10 μm from the nuclear border in two separate pulling experiments (i.e. in different cells under similar conditions).

2. When the pipette is placed 10 μm from the nuclear border, measure induced strains in the direction of pull in the cytoplasm adjacent to the pipette (0–5.5 μm from the tip), in distal cytoplasm adjacent to the nucleus (5–10 μm away), and in the proximal portion of the nucleus (10–15 μm away).
3. Perform identical measurements in similarly treated cells with a pipette placed 5 μm from the nuclear border to determine strains at the same distances (0–5, 5–10, or 10–15 μm) from the pipette tip and hence, under similar stress. These locations now fall in the cytoplasm adjacent to the nucleus, in the proximal nucleus, and in the distal nucleus, respectively (*Figure 9*).
4. Calculate the ratio of nuclear to cytoskeletal stiffness by determining the ratio of strains measured in the adjacent cytoplasm and proximal nucleus (i.e. 5–10 μm away from pipettes placed 10 μm and 5 μm away from the nuclear border, respectively), according to the equations described in *Figure 9*.
5. To measure apparent Poisson's ratios, harpoon the cells 10 μm from the nuclear envelope and pull the pipette 5 μm away from the nuclear border. Calculate the ratio of the strain (per cent changes in distances between different phase-dense particles in cytoplasm or nucleus) before and after stress application in the region along the axis perpendicular to the direction of pull divided by the strain in the direction of pull. All strains are measured in equal areas (9 μm^2), equally distant (4–5 μm) from both the pipette and the nuclear border, and all displacements should be of equal magnitude. Note: Poisson's ratio calculated in this manner must be viewed as an 'apparent' rather than absolute value, because the ratio is based on a two-dimensional projection of a three-dimensional material in cells adherent to an underlying solid substrate.

2.6 Analysing chromosomal connectivity and mechanics

Our work on mechanical connectivity in living cells suggested the existence of a continuous filamentous network within the nucleus as well as in the cytoplasm (37). To test directly whether discrete networks physically interlink chromatin in the nucleus, we used very fine glass microneedles (tips less than 0.5 μm diameter) to harpoon individual nucleoli within cultured interphase cells or individual chromosomes in mitotic cells. Using this approach, we found that pulling a single nucleolus or chromosome out from interphase or

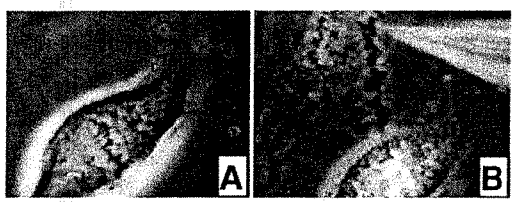

Figure 10. Microsurgical analysis of chromatin structure. A mitotic endothelial cell before (A) and after (B) a single chromosome was harpooned and removed from the cell using a micromanipulator. Note that pulling on one chromosome results in sequential removal of all the other chromosomes, revealing mechanical connectedness in the entire genome.

mitotic cells resulted in sequential removal of the remaining nucleoli and chromosomes, interconnected by a continuous elastic thread (40) (*Figure 10*). Enzymatic treatments of interphase nucleoplasm and chromosome chains held under tension revealed that mechanical continuity within the chromatin was mediated by DNA. Furthermore, when ion concentrations were raised and lowered, both the chromosomes and the interconnecting strands underwent multiple rounds of decondensation and recondensation (39–41). Fully decondensed chromatin strands also could be induced to recondense into chromosomes with pre-existing size, shape, number, and position by adding antibodies against histone H1 or topoisomerase II alpha, but not other nuclear proteins (39–40). These data suggest that DNA, its associated protein scaffolds, and surrounding cytoskeletal networks function as a structurally unified system. Mechanical coupling within the nucleoplasm may co-ordinate dynamic alterations in chromatin structure, guide chromosome movement, and ensure fidelity of mitosis. A typical assay is presented in *Protocol 13*.

Protocol 13. Analysis of chromatin mechanics and dynamics

Equipment and reagents

- See *Protocols 10* and *11*
- Glass coverslips
- Microscope
- 60 mM $MgCl_2$; trypsin; proteinase K

Method

1. Culture cells on glass coverslips in standard serum-containing medium. We have used endothelial cells and fibroblasts (39–41).
2. Transfer the coverslip to the lid of a 35 mm Petri dish covered with 2 ml serum-free medium with Hepes pH 7.4 and position on the stage of a Diaphot inverted microscope. For studies involving oil-immersion, use a cell culture chamber with a glass coverslip bottom, instead of 35 mm dish lid.

3. Fabricate the microneedle (0.5 μm wide tip), using methods in *Protocols 10* and *11*, and position it with the micromanipulator above a nucleolus or the edge of a mitotic plate.
4. Rapidly introduce the microneedle into the cell in a single motion and 'harpoon' an individual nucleolus or chromosome by gently touching it with the tip of the needle.
5. Pull out the nucleolus or chromosome attached to the microneedle through the original micropuncture opening made in the cell membrane by reversing the direction of pipette movement using the micromanipulator. The remaining chromatin strand will follow forming a continuous, elastic 'chain'. Note: the chromatin chain can be held in an extended form for study by either holding the micromanipulator in place or adhering the distal end of the chain to another cell or the surface of the culture dish by gently pressing the pipette against the surface. The connectivity between chromosomes can be studied by using the micropipette to apply a mechanical force directly to chromosome chains.
6. Probe the effect of different ions, chemicals, or biological compounds on chromatin mechanics and dynamics by placing a droplet (2 μl) containing the compound of interest directly above the isolated chain, or by replacing the original medium with the compound at the desired final concentration.
7. To analyse chromosome dynamics, incubate the extended chromosome chain with high salt, such as 60 mM $MgCl_2$ or place a 2 μl droplet of protease, such as the combination of trypsin (5 μg) and proteinase K (50 μg) above the isolated chain. The chromosomes will unfold and become phase lucent within seconds. These dynamic effects are reversible upon the return to the original ionic conditions or after addition of molecules involved in chromosome compaction (e.g. histone H1). Note: caution should be used during the handling of unfolded chromosomes, because excessive fluid turbulence can easily disrupt their pattern, entangle them, or cause non-specific sticking to the substrate. A more thorough description of methods and materials used to study chromosome dynamics *in situ* may be found in our recent publications (39–41).

3. Conclusion

In this chapter, we review a variety of different techniques that we have developed to manipulate and probe cell structure and cytoskeletal signalling. Our initial working hypothesis, based on a model of cellular tensegrity, suggested that cell form and function may be largely controlled based on

mechanical interactions between cells and their ECM. Our initial methods for varying cell–ECM interactions in a controlled manner were consistent with this model, because they showed tight coupling between cell spreading and growth. However, we could not discriminate signals triggered by cell shape modulation from signalling induced by local integrin receptor binding and clustering. In fact, by developing a microbead technique for inducing integrin clustering independently of cell spreading we could confirm that integrin binding alone is sufficient to activate many chemical signalling pathways that are involved in cellular control. Furthermore, we showed that much of this signalling occurs on the cytoskeleton at the site of integrin binding to the backbone of the FAC.

Nevertheless, when we finally developed a method to separate local cell–ECM binding events from cell spreading using micropatterned substrates, we discovered that cell shape exerts separate and distinct regulatory signals that act many hours after initial integrin and growth factor receptor signalling events to control cell cycle progression. In addition, we developed various other techniques to probe cell structure which revealed that the cell is indeed 'hard-wired' to respond to mechanical stresses; that cell surface adhesion receptors provide preferred sites for transmembrane mechanical transfer; and that living cells behave as if they are tensegrity structures when they are mechanically stressed. Taken together, these new methods have led to a new view of cell regulation based on tensegrity architecture in which mechanics and chemistry are tightly coupled. Better understanding of how cells control their shape and function will require development of more techniques that incorporate methods for controlling and quantitating changes in cell structure as well as biochemical events.

Acknowledgements

We would like to acknowledge the invaluable technical assistance of Deborah Flusberg, Adi Loebl, and Paul Kim, and thank Ruth L. Capella and Jeanne Nisbet for careful reading and editing of the manuscript. We would also like to thank Dr George Whitesides and the members of his group for their help in developing the micropatterning technique. This work was supported by grants from NIH, NASA, NSF, DOD, and NATO.

References

1. Ingber, D. E., Madri, J. A., and Jamieson, J. D. (1981). *Proc. Natl. Acad. Sci. USA*, **78**, 390.
2. Ingber, D. E. and Jamieson, J. D. (1985). In *Gene expression during normal and malignant differentiation* (ed. L. C. Andersson, C. G. Gahmberg, and P. Ekblom), p. 13. Academic Press, Orlando.
3. Ingber, D. E. (1993). *J. Cell Sci.*, **104**, 613.

4. Ingber, D. E. (1997). *Annu. Rev. Physiol.*, **59**, 575.
5. Ingber, D. E. (1998). *Sci. Am.*, **278**, 48.
6. Ingber, D. E. (1991). *Curr. Opin. Cell Biol.*, **3**, 841.
7. Ingber, D. E. (1993). *Cell*, **75**, 1249.
8. Ingber, D. E. (1990). *Proc. Natl. Acad. Sci. USA*, **87**, 3579.
9. Ingber, D. E. and Folkman, J. (1989). *J. Cell Biol.*, **109**, 317.
10. Mooney, D., Hansen, L., Farmer, S., Vacanti, J., Langer R., and Ingber, D. E. (1992). *J. Cell. Physiol.*, **151**, 497.
11. Lee, K.-M., Tsai, K., Wang, N., and Ingber, D. (1998). *Am. J. Physiol.*, **274**, H76.
12. Huang, S., Chen, C. S., and Ingber, D. E. (1998). *Mol. Biol. Cell*, **9**, 3179.
13. Folkman, J. and Moscona, A. (1978). *Nature*, **273**, 345.
14. Katz, B. Z. and Yamada, K. M. (1997). *Biochimie*, **79**, 467.
15. Schwartz, M. A., Lechene, C., and Ingber, D. E. (1991). *Proc. Natl. Acad. Sci. USA*, **88**, 7849.
16. Plopper, G. and Ingber, D. E. (1993). *Biochem. Biophys. Res. Commun.*, **193**, 571.
17. Plopper, G., McNamee, H., Dike, L. E., Bojanowski, K., and Ingber, D. E. (1995). *Mol. Biol. Cell*, **6**, 1349.
18. McNamee, H., Liley, H., and Ingber, D. E. (1996). *Exp. Cell Res.*, **224**, 116.
19. Miyamoto, S., Teramoto, H., Coso, O. A., Gutkind, J. S., Burbelo, P. D., Akiyama, S. K., *et al.* (1995). *J. Cell Biol.*, **131**, 791.
20. Burr, J. G., Dreyfuss, G., Penman, S., and Buchanan, J. M. (1980). *Proc. Natl. Acad. Sci. USA*, **77**, 3484.
21. Dike, L. E. and Ingber, D. E. (1996). *J. Cell Sci.*, **109**, 2855.
22. Xia, Y., Mrksich, M., Kim, E., and Whitesides, G. M. (1995). *J. Am. Chem. Soc.*, **117**, 9576.
23. Wilbur, J. L., Kim, E., Xia, Y., and Whitesides, G. M. (1995). *Adv. Mater.*, **7**, 649.
24. Singhvi, R., Kumar, A., Lopez, G. B., Stephanopoulos, G. N., Wang, D. I. C., Whitesides, G. M., *et al.* (1994). *Science*, **264**, 696.
25. Chen, C. S., Mrksich, M., Huang, S., Whitesides, G. M., and Ingber, D. E. (1997). *Science*, **276**, 1425.
26. Dike, L. E., Chen, C. S., Mrkisch, M., Tien, J., Whitesides, G., and Ingber, D. E. (1999). *In Vitro*, in press.
27. Wang, N., Butler, J. P., and Ingber, D. E. (1993). *Science*, **260**, 1124.
28. Wang, N. and Ingber, D. E. (1994). *Biophys. J.*, **66**, 2181.
29. Wang, N. and Ingber, D. E. (1995). *Biochem. Cell Biol.*, **73**, 327.
30. Wang, H. (1998). *Hypertension*, **32**, 162.
31. Potard, U. S., Butler, J. P., and Wang, N. (1997). *Am. J. Physiol.*, **272**, C1654.
32. Ezzell, R. M., Goldmann, W. H., Wang, N., Parasharama, N., and Ingber, D. E. (1997). *Exp. Cell Res.*, **231**, 14.
33. Goldmann, W. H., Galneder, R., Ludwig, M., Xu, W., Adamson, E. D., Wang, N., *et al.* (1998). *Exp. Cell Res.*, **239**, 235.
34. Yoshida, M., Westlin, W. F., Wang, N., Ingber, D. E., Rosenzweig, A., Resnick, N., *et al.* (1996). *J. Cell Biol.*, **133**, 445.
35. Pourati, J., Maniotis, A., Spiegel, D., Schaffer, J. L., Butler, J. P., Fredberg, J. J., *et al.* (1998). *Am. J. Physiol.*, **274**, C1283.
36. Chicurel, M. E., Singer, R. H., Meyer, C. J., and Ingber, D. E. (1998). *Nature*, **392**, 730.

37. Maniotis, A. J., Chen, C. S., and Ingber, D. E. (1997). *Proc. Natl. Acad. Sci. USA*, **94**, 849.
38. Eckes, B., Dogic, D., Colucci-Guyon, E., Wang, N., Maniotis, A. J., Ingber, D., *et al.* (1998). *J. Cell Sci.*, **111**, 1897.
39. Maniotis, A. J., Bojanowski, K., and Ingber, D. E. (1997). *J. Cell Biochem.*, **65**, 114.
40. Bojanowski, K., Maniotis, A. J., Plisov, S., Larsen, A. K., and Ingber, D. E. (1998). *J. Cell Biochem.*, **69**, 127.
41. Bojanowski, K. and Ingber, D. E. (1998). *Exp. Cell Res.*, **244**, 286.

A1

List of suppliers

Adam and List Associates, 110 Shames Drive, Westbury, NY 11590, USA.

Amersham

Amersham International plc., Lincoln Place, Green End, Aylesbury, Buckinghamshire HP20 2TP, UK.

Amersham Corporation, 2636 South Clearbrook Drive, Arlington Heights, IL 60005, USA.

Amicon Ltd., distributed by Millipore, Upper Mill, Stone House, Gloucestershire GL20 2BJ, UK.

Anderman

Anderman and Co. Ltd., 145 London Road, Kingston-Upon-Thames, Surrey KT17 7NH, UK.

BDH, Merck Ltd., Hunter Boulevard, Magna Park, Lutterworth, Leicestershire LE17 4XN, UK.

Beckman Instruments

Beckman Instruments UK Ltd., Oakley Court, Kingsmead Business Park, London Road, High Wycombe, Bucks HP11 1J4, UK.

Beckman Instruments Inc., PO Box 3100, 2500 Harbor Boulevard, Fullerton, CA 92634, USA.

Becton Dickinson

Becton Dickinson and Co., Between Towns Road, Cowley, Oxford OX4 3LY, UK.

Becton Dickinson and Co., 2 Bridgewater Lane, Lincoln Park, NJ 07035, USA.

Becton Dickinson, Collaborative Biomedical Products, 2 Oak Park, Bedford, MA 01730, USA..

Becton Dickinson Labware, Falcon, Franklin Lakes, NJ 07417, USA.

Bio

Bio 101 Inc., c/o Statech Scientific Ltd, 61–63 Dudley Street, Luton, Bedfordshire LU2 0HP, UK.

Bio 101 Inc., PO Box 2284, La Jolla, CA 92038–2284, USA.

Bio-Rad Laboratories

Bio-Rad Laboratories Ltd., Bio-Rad House, Maylands Avenue, Hemel Hempstead HP2 7TD, UK.